

Article

Probing Low-Temperature OCM Performance over a Dual-Domain Catalyst Bed

Baoting Huang, Jin Wang, Dina Shpasser and Oz M. Gazit * 

Faculty of Chemical Engineering, Technion-Israel Institute of Technology, Haifa 3200003, Israel

* Correspondence: ozg@technion.ac.il

Abstract: The Mn-Na₂WO₄/SiO₂ catalyst is regarded as the most promising catalyst for the oxidative coupling of methane (OCM). Despite its remarkable performance, the Mn-Na₂WO₄/SiO₂ catalyst requires a high reaction temperature (>750 °C) to show significant activity, a temperature regime that simultaneously causes quick deactivation. In the current work, we show that the benefits of this catalyst can be leveraged even at lower reaction temperatures by using a stacked catalyst bed, which includes also a small amount of 5% La₂O₃/MgO on-top- of the Mn-Na₂WO₄/SiO₂ catalyst. The simple stacking of the two catalysts provides >7-fold higher activity and ~1.4-fold higher C₂ yield at 705 °C compared to Mn-Na₂WO₄/SiO₂ and La₂O₃/MgO, respectively. We specifically show that the enhanced OCM performance is associated with synergistic interactions between the two catalyst domains and study their origin.

Keywords: low temperature activation; mixed-bed catalysts; OCM; Mn-Na₂WO₄/SiO₂; La₂O₃; deactivation



Citation: Huang, B.; Wang, J.; Shpasser, D.; Gazit, O.M. Probing Low-Temperature OCM Performance over a Dual-Domain Catalyst Bed. *Chemistry* **2023**, *5*, 1101–1112. <https://doi.org/10.3390/chemistry5020075>

Academic Editors: José Antonio Odriozola and Hermenegildo García

Received: 15 March 2023
Revised: 4 May 2023
Accepted: 5 May 2023
Published: 8 May 2023



Copyright: © 2023 by the authors. Licensee MDPI, Basel, Switzerland. This article is an open access article distributed under the terms and conditions of the Creative Commons Attribution (CC BY) license (<https://creativecommons.org/licenses/by/4.0/>).

1. Introduction

The oxidative coupling of methane (OCM) reaction was identified by Keller and Bhasin in 1983 as a promising route to convert methane directly into ethane and ethylene [1]. If this process can be accomplished in an effective small-scale and distributed way, it can be used to convert methane from natural gas, shale gas [2], biogas [3], and landfills into important value-added products such as polymers. However, due to the symmetric CH₄ and the strong C-H bonds, a high reaction temperature is usually required to promote OCM (>750 °C) [1]. The high reaction temperature also promotes the over-oxidation of methane into CO_x (CO and CO₂) and affects the longevity of the catalyst over prolonged exposure [4]. Despite extensive efforts, a catalyst of industrially applicable yield and high stability has not yet been found.

The Mn-Na₂WO₄/SiO₂ (MnNaWSi) catalyst has been and is still regarded as the most promising catalyst for this reaction, with early reports showing CH₄ conversion ~25% with a C₂ selectivity of ~80% (>800 °C) over long periods of time (~500 h) [5,6]. Despite the remarkable performance of the MnNaWSi catalyst, more recent reports show that structural changes in the multi-metal oxide material occur under reaction conditions [6–14]. Hayek et al. have shown that these structural changes also occur in the presence of additional dopants and result in strong deactivation, which is masked by the use of large amounts of catalyst [15]. Distinctly, it is the melting of crystalline Na₂WO₄ at 698 °C that is believed to impose instability in the catalyst structure due to its strong interaction with the silica support and the MnO_x phase as well as its evaporation (~1000 °C) at hotspots in the catalyst bed [8,16]. An operating temperature below or close to 700 °C should in principle limit those structural changes and help suppress the over-oxidation of the desired C₂ products into CO₂ [17].

It is generally accepted that the activation of the reaction involves the cleavage of the C-H bond to form methyl radicals (CH₃•). The CH₃• then couples to form ethane in the

gas phase near the catalyst's surface [4,14,16,18]. It has been shown that the production rate of methyl radicals is strongly correlated to the C₂ yield [19–21]. Ideally, a good OCM catalyst would be able to generate methyl radicals at low temperatures (below 700 °C) and allow those to desorb and couple in the gas phase [14,20,21]. Hence, it is the ability of the MnNaWSi catalyst to generate and release methyl radicals that enable its remarkably high C₂ selectivity [14]. However, the MnNaWSi catalyst is only able to effectively activate methane above 750–800 °C, which makes the produced C₂ products highly susceptible to further oxidation to unwanted CO_x.

Lansford and coworkers showed that lanthanum oxide (La₂O₃) is active for OCM and is able to generate CH₃• even at temperatures as low as ~500 °C [20,22]. However, the C₂ selectivity of the La₂O₃ is relatively low compared to the MnNaWSi catalyst, which limits its applicability on its own. Hence, the combination of La₂O₃ and the MnNaWSi catalyst should produce a superior low-temperature OCM catalyst. Wu et al. reported using La to dope the MnNaWSi catalyst to achieve enhanced dispersion of the Mn and W on the silica support [23], along with a significant improvement in C₂ selectivity and activity in OCM. Whereas Ghose et al. and Ismagilov et al., showed only a marginal enhancement in C₂ selectivity, following a similar catalyst doping procedure [24,25]. Neither of them reported low temperature reaction performance. Nevertheless, at present, there is a consensus in the OCM literature that supports the high potential of La₂O₃ to reduce OCM reaction temperature [22,26–29]. Recently, Jaroenpanon et al. showed that Mn-Na₂WO₄ supported on La₂O₃, rather than on the commonly used SiO₂ support, provided a C₂ yield of 5~10% between 500 and 650 °C [30]. Zou et al. reported a ~32% C₂ selectivity and a C₂ yield of ~10% at 550–700 °C over a catalyst bed composed of a 1:1 (%wt) mechanical mixture of La₂O₃ and Na₂WO₄/SiO₂ (NaWSi) [31]. However, the economic benefit of using the rare earth La₂O₃ as a bulk support material for OCM is questionable [9,14,15]. In this study, we evaluate the OCM performance over MnNaWSi mechanically mixed with a small amount (~0.6 wt.%) of La₂O₃ nanoparticles supported on MgO (La/MgO). The small amount of La is shown to provide significant OCM enhancement with the MgO support mitigating the deactivation by limiting the direct interaction of the Na₂WO₄ melt with the La₂O₃. We demonstrate that the La/MgO to MnNaWSi weight ratio in the catalyst bed has a strong effect on catalytic performance. We further compared the effect of mixing the two catalysts vs. stacking the La/MgO catalyst on-top of the MnNaWSi. The effect of the above configuration on catalytic performance and catalyst deactivation at low-temperature reaction is discussed in detail.

2. Experimental Procedures

2.1. Catalyst Preparation

Mn₂O₃-Na₂WO₄/SiO₂ (MnNaWSi). The Mn₂O₃-Na₂WO₄/SiO₂ was synthesized following a multi-step incipient wetness impregnation (IWI) as described in detail elsewhere [12,15]. Prior to synthesis, fumed silica of 7 nm primary particle size (Sigma-Aldrich, St. Louis, MO, USA) was dried in an oven at 140 °C for 12 h. Firstly, 1.4 mL of aqueous solution (miliQ water) of Mn(Ac)₂·4H₂O (Sigma-Aldrich) with an appropriate concentration was dropwise added to 1 g of silica while vortex mixing. After impregnation, the powder was sufficiently mixed and then dried in the oven at 140 °C overnight. After drying, the powder was calcined to obtain Mn₂O₃/SiO₂. The calcination was conducted in a tubular furnace, under air flow of ~60 mL·min⁻¹ at 110 °C for 2 h and then at 500 °C for 3 h. The ramping rate was set to 2 °C per minute. Next, 1.4 mL solution of Na₂WO₄·2H₂O (Alfa Aesar, Haverhill, MA, USA) in miliQ water with appropriate concentration was impregnated in the same way on the obtained Mn₂O₃/SiO₂. After drying in the oven at 140 °C overnight, the catalyst was calcined in a tubular furnace, under air flow of ~60 mL·min⁻¹ at 115 °C for 2 h and then at 850 °C for 5 h. The ramping rate was set to 5 °C per minute.

La/MgO. The La/MgO was synthesized by IWI. Prior to synthesis, the MgO of 325 mesh particle size (Strem Chemicals, Inc., Newburyport, MA, USA) was dried in an oven at 140 °C for 12 h. An amount of 1 mL of aqueous solution (miliQ water) of

$\text{La}(\text{NO}_3)_3 \cdot 6\text{H}_2\text{O}$ (Strem Chemicals, Inc.) with an appropriate concentration was dropwise added to 1 g of MgO while vortex mixing. After impregnation, the powder was sufficiently mixed and then dried in the oven at 140 °C overnight. After drying, the powder was calcined to obtain La/MgO. The calcination was conducted in a tubular furnace, under air flow of $\sim 60 \text{ mL} \cdot \text{min}^{-1}$ at 800 °C for 4 h. The ramping rate was set to 5 °C per minute.

La_2O_3 . The La_2O_3 was synthesized by the thermal decomposition of $\text{La}(\text{NO}_3)_3 \cdot 6\text{H}_2\text{O}$ (Strem Chemicals, Inc.) at 115 °C for 2 h and 700 °C for 4 h. The ramping rate was set at 5 °C per minute.

2.2. Characterization Methods

The loading of the metals in each sample was determined by Inductively Coupled Plasma-Optical Emission Spectroscopy (ICP-OES) using a Thermo Scientific (iCAP 6000) spectrometer. Prior to analysis, each sample was dissolved in HNO_3 and HCl in 1/4 volumetric mixture at 70 °C overnight and then diluted with miliQ water. Crystalline components of the catalysts were determined by Powder X-ray Diffraction (PXRD). Patterns were recorded at ambient conditions on a Rigaku SmartLab diffractometer using $\text{Cu K}\alpha$ radiation ($\lambda = 1.54 \text{ \AA}$) with 3° min^{-1} scan speed and 0.01° angle step. The catalyst morphology was evaluated before and after the reaction using High-Resolution Scanning Electron Microscopy (HR-SEM). The analysis was performed on an Ultraplus (Carl Zeiss, Heidelberg, Germany) Microscope. Everhart-Thornley and Backscattering detectors were used. For analysis, the sample powder was sprinkled on a carbon film before imaging.

2.3. Catalytic Testing

The catalysts were tested using a single-pass fixed-bed flow reactor made of quartz with an inner diameter of 7 mm. In each run of reaction, 50 mg of catalyst was loaded and packed inside the reactor. Two pieces of quartz wool were loaded and packed on both ends of the catalyst bed like a sandwich configuration to stabilize the reactor bed. Prior to catalyst loading, the sample was sieved and collected within 60–100 mesh. The reactor bed was packed to be 5 mm long. As La_2O_3 and MgO support were denser than SiO_2 , some amount of inert quartz sand (60–100 mesh) was added and mixed with the reactor bed to reach a consistent bed size. The temperature of the quartz reactor was controlled by a temperature-controlled split tubular furnace (Vecstar, Eurotherm, Suisse). The feed gas temperature was monitored by an external K-type thermocouple housed in a quartz capillary tube. The thermocouple was placed above the catalyst bed inside the reactor. It is noted that the measured furnace temperature was consistently higher by $\sim 10^\circ \text{C}$; hence, for convenience, we note only the furnace temperature. The feed gas composition and flow rate were controlled by mass flow controllers (Brooks SLA5850). Typically, the feed gas mixture had a total flow of 50 mL min^{-1} STP with composition of 4:1:1:4 $\text{CH}_4:\text{O}_2:\text{N}_2:\text{Ar}$, which resulted in GHSV (gas hourly space velocity) of $60,000 \text{ mL h}^{-1} \text{ g}^{-1}$ (unless otherwise stated upon total flow change). The absolute reactor pressure was kept constant at ~ 1.3 bar using a back-pressure controller (Brooks SLA5820). The reaction-produced water was separated in an ice trap placed at the outlet of the reactor. The outlet stream of the reactor was analyzed by a Clarus 580 GC (PerkinElmer) equipped with TCD and FID detectors. The CH_4 and O_2 conversions were calculated according to Equation (1) (i denotes CH_4 or O_2), while C_2 selectivity and C_2 yield were calculated according to Equation (2) (F_i is molar flow rate) and Equation (3). To consider the change in the molar flow following the reaction, N_2 was used as an internal standard. The mass balance was ensured to close with $>95\%$.

$$\text{Conversion}(\%) = \frac{F_{i,\text{in}} - F_{i,\text{out}}}{F_{i,\text{in}}} \cdot 100 \quad (1)$$

$$\text{C}_2 \text{ Selectivity}(\%) = \frac{2 \cdot (F_{\text{C}_2\text{H}_4} + F_{\text{C}_2\text{H}_6})}{F_{\text{CH}_4,\text{in}} - F_{\text{CH}_4,\text{out}}} \cdot 100 \quad (2)$$

$$C_2 \text{ yield}(\%) = CH_4 \text{ Conversion}(\%) \cdot C_2 \text{ Selectivity}(\%) / 100 \quad (3)$$

The stacking and mixing of different catalytic beds were prepared as follows:

Stacked Beds (s). The stacking (s) beds La_2O_3 -MnNaWSi and La/MgO-MnNaWSi were prepared by packing the La-containing catalysts (La_2O_3 or La/MgO) on top of the already packed MnNaWSi catalyst bed. Different bed ratios (x) between the La-containing bed and the entire bed (50 mg) were studied, denoted as La_2O_3 -MnNaWSi_{xs} and La/MgO-MnNaWSi_{xs} (x = 0.1, 0.2, or 0.5), respectively. The catalyst bed size for all tests was kept constant at length of 5 mm. Since La_2O_3 and La/MgO have higher density than the MnNaWSi catalyst, the MnNaWSi catalyst bed was diluted with inert quartz sand (60–100 mesh) to maintain a consistent bed size of 5 mm. The quartz sand was mixed with MnNaWSi bed instead of La catalyst beds to minimize the limitation of $\bullet CH_3$ transport to the lower bed. Prior to the preparation of catalyst bed, all particles were sieved and collected in between 60 and 100 mesh.

Mixed Beds (m). The mechanically mixed (m) beds of La_2O_3 -MnNaWSi and La/MgO-MnNaWSi were prepared by mixing the La-containing catalysts (La_2O_3 or La/MgO) with MnNaWSi. Prior to mixing, all particles were sieved and collected in between 60 and 100 mesh. Different weight ratios (x) between the La-containing catalysts and the entire bed (50 mg) were studied, denoted as La_2O_3 -MnNaWSi_{xm} and La/MgO-MnNaWSi_{xm} (x = 0.1, 0.2 and 0.8), respectively. The catalyst beds for all tests were kept constant at mass of 50 mg and length of 5 mm. Since La_2O_3 and La/MgO have higher density than the MnNaWSi catalyst, the MnNaWSi catalyst bed was diluted with inert quartz sand (60–100 mesh) to maintain a consistent bed size of 5 mm.

3. Results and Discussion

The catalysts in this study include La_2O_3 , MgO-supported La_2O_3 (La/MgO), and Mn- Na_2WO_4 - SiO_2 (MnNaWSi) or a combination thereof. We examined two types of catalyst bed packing: (1) stacking (s), namely the La-containing catalyst (La_2O_3 or La/MgO) placed on top of the MnNaWSi catalyst bed, and (2) mixed (m), namely a uniform mechanical mix of La-containing catalyst (La_2O_3 or La/MgO) and the MnNaWSi. For clarity, the nomenclature of all the reactor bed combination tested was summarized in Table 1. Different loadings of the La-containing bed (La catalyst mass fraction in bed) were studied, as shown in Table 1. Each catalyst alone, La_2O_3 , La/MgO, or MnNaWSi was tested separately as controls.

Table 1. Nomenclature and the description of the catalyst reactor bed, including its reactor bed configuration and the weight proportion of the La bed.

Name	Nomenclature	La Catalyst Mass Fraction in Bed
	La/MgO	–
	La_2O_3	–
	MnNaWSi	–
La_2O_3 + MnNaWSi	La_2O_3 -MnNaWSi _{0.1s}	0.1
	La/MgO-MnNaWSi _{0.1s}	0.1
	La/MgO-MnNaWSi _{0.2s}	0.2
La/MgO + MnNaWSi	La/MgO-MnNaWSi _{0.5s}	0.5
	La/MgO-MnNaWSi _{0.1m}	0.1
	La/MgO-MnNaWSi _{0.2m}	0.2
	La/MgO-MnNaWSi _{0.8m}	0.8

where 's' and 'm' represent a stacked and mixed-bed configuration, respectively.

3.1. Catalyst Characterization

The loadings of the active metals in the La/MgO and the MnNaWSi catalysts were measured by ICP-OES, and the results are summarized in Table S1. The crystal phases identified for MnNaWSi were cubic Na_2WO_4 , tetragonal α -cristobalite, and tetragonal $\text{Mn}_7\text{O}_8\text{SiO}_4$, consistent with the literature of Mn_2O_3 - Na_2WO_4 - SiO_2 , as shown in Figure S1 [10,15,32,33]. The crystal phases of La/MgO were cubic MgO and hexagonal $\text{La}(\text{OH})_3$, as shown in Figure S1a. Notably, the La_2O_3 phase is prone to react with the moisture in the air. Since the catalyst samples were exposed to ambient air containing water moisture, the spectra of the La-containing samples also showed the formation of $\text{La}(\text{OH})_3$, as shown in Figure S1b in Supplementary Materials. To validate the formation of La_2O_3 , we analyzed a dedicated fresh catalyst sample, which was analyzed immediately as prepared using PXRD, as shown in Figure S1c. Previous work reported that at around 500 °C under air, the $\text{La}(\text{OH})_3$ phase transforms into La_2O_3 [34]. Hence, it is assumed that because of the in-situ calcination, the reaction temperature (>650 °C), and the oxidative conditions of OCM, the La in the active catalyst bed was initially present as La_2O_3 in both the La/MgO and La_2O_3 catalysts.

3.2. Catalytic Performance

The reaction onset temperature was ~700 °C for the MnNaWSi catalyst and <650 °C for the La/MgO catalyst in Figure 1a. Interestingly, by simply stacking a small amount of the La/MgO catalyst (10 wt.% of the bed) over the MnNaWSi catalyst (La/MgO-MnNaWSi_0.1s), the reaction started already below 650 °C, as shown in Figure 1a. Even more interesting is the higher C_2 selectivity and C_2 yield obtained by the La/MgO-MnNaWSi_0.1s, as shown in Figure 1c,d.

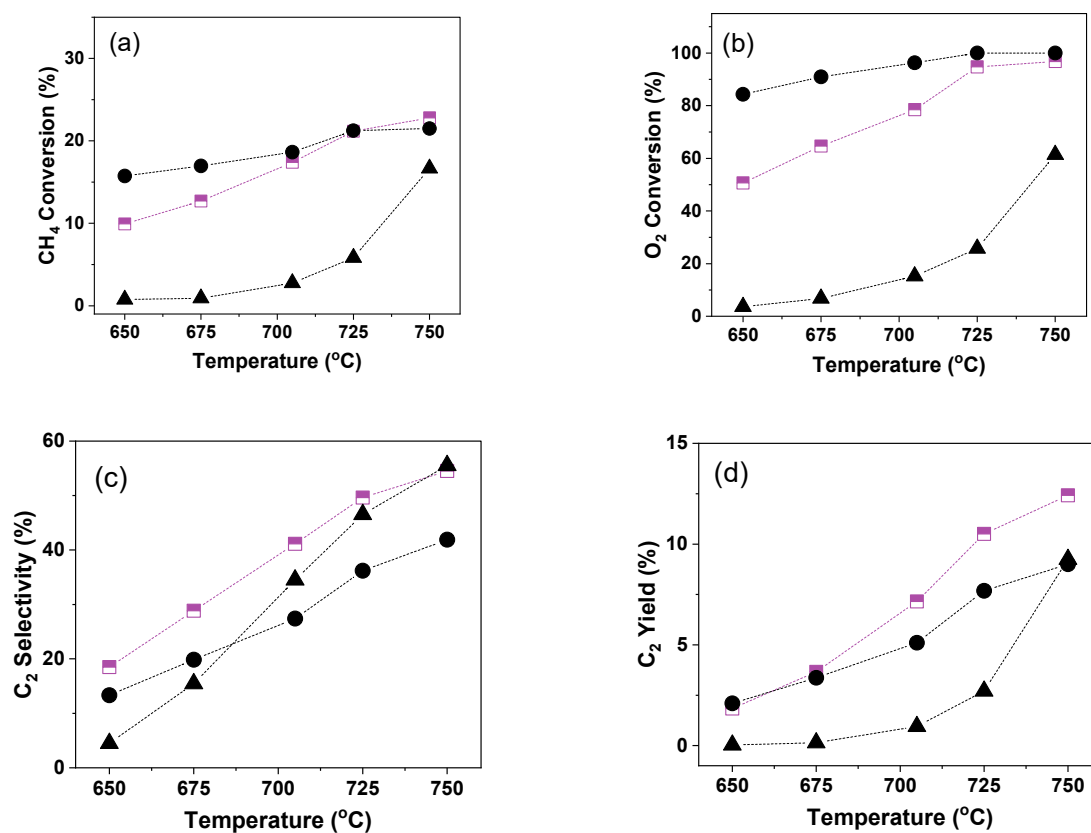


Figure 1. Temperature dependencies (650–750 °C) of the La/MgO, MnNaWSi catalysts, and the stacking experiment, La/MgO-MnNaWSi_0.1s. (a) CH₄ conversion; (b) O₂ conversion; (c) C₂ selectivity; and (d) C₂ yield. ■ La/MgO-MnNaWSi_0.1s, • La/MgO, and ▲ MnNaWSi. Stacking of La/MgO and MnNaWSi beds with 10 wt.% of La/MgO and 90 wt.% of MnNaWSi.

The low activity of the MnNaWSi catalyst below 750 °C is consistent with previously published observations [35–37]. The drastic increase in activity of the MnNaWSi above 750 °C was previously associated with its ability to desorb molecular oxygen [37], facilitated by the interactions between the MnO_x and the Na₂WO₄ phases [10,38]. Gordienko et al. showed that the onset temperature for O₂ desorption from the MnNaWSi catalyst was 700 °C and reached a maximum of around 750–800 °C [37]. Using operando Raman and XRD-CT, Werny and Matras et al. demonstrated that at temperatures > 650 °C, the Mn₇O₈SiO₄ phase starts losing its crystallinity due to reaction with the molting Na₂WO₄ and the simultaneous formation of MnWO₄ [10,38]. These coincide with the strong deactivation of the MnNaWSi catalyst, as was previously addressed by Lunsford and coworkers [39] and later on emphasized by Hayek et al. [15]. Hence, from the perspective of the longevity of the MnNaWSi catalyst, it is beneficial to run the OCM reaction at a temperature lower than the melting temperature of Na₂WO₄ (698 °C).

We found that the CH₄ conversion over the La/MgO catalyst increased only slightly (~16–21%) as compared to the more significant increase in MnNaWSi (1–16%), but the C₂ selectivity of La/MgO did increase with temperature, as shown in Figure 1a,c, respectively. The La/MgO-MnNaWSi_0.1s catalyst showed C₂ selectivity greater or similar to that of the MnNaWSi, which comprises 90 wt.% of the catalyst bed, as shown in Figure 1c. However, its conversion was comparable to that of the La/MgO catalyst, which comprises only 10 wt.% of the La/MgO-MnNaWSi_0.1s catalyst bed. Specifically, at 725 °C, we find that the CH₄ and O₂ conversions of the La/MgO-MnNaWSi_0.1s were the same as those of the La/MgO while the selectivity of the former was higher by 14% and even slightly higher than that of the MnNaWSi. The reaction results at 725 °C with time on stream for 7 h demonstrate that the performance of all three catalysts was stable, with the C₂ yield being consistently highest over the La/MgO-MnNaWSi_0.1s, as shown in Figure 2d.

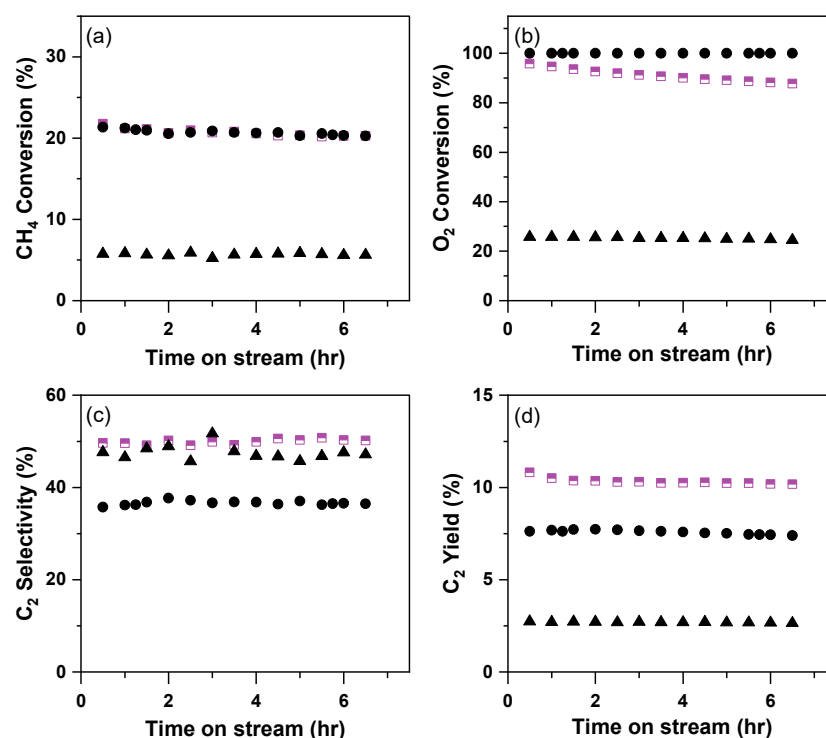


Figure 2. Catalytic performance at low temperature (725 °C) of single catalyst beds and composite bed. (a) CH₄ conversion; (b) O₂ conversion; (c) C₂ selectivity; and (d) C₂ yield. • La/MgO, ▲ MnNaWSi, and ■ La/MgO-MnNaWSi_0.1s.

The benefit of mixing bulk La₂O₃ with Na₂WO₄/SiO₂ (NaWSi) at a 50:50 wt.% ratio was previously identified by Zou et al. [31]. Their results at ~725 °C show similar performance between the La₂O₃ and the La₂O₃ mixed with Na₂WO₄/SiO₂, which indi-

cates that the La_2O_3 phase at that temperature range was governing the catalytic performance. We, therefore, tested OCM using unsupported La_2O_3 stacked on MnNaWSi at a 10:90 wt.% (La-MnNaWSi_0.1s) at 725 °C and compared it to the performance of the La/MgO-MnNaWSi_0.1s catalyst, as shown in Figure S2. Given that MgO gives a very low C_2 yield (Figure S2), it can be expected that the La-MnNaWSi_0.1s, having ~30 fold more La_2O_3 , would give significantly higher activity and C_2 yield compared to the La/MgO-MnNaWSi_0.1s catalyst. Interestingly, it was observed that over the relatively short reaction time (7 h), the C_2 yield of the former started dropping while the latter remained fairly stable (Figure S2d). The most evident difference between the two catalysts was in the sharper decrease in O_2 conversion of the La/MgO-MnNaWSi_0.1s compared to La-MnNaWSi_0.1s. We associate the leveling in the C_2 yield in the former with the decrease in O_2 gas phase concentration, which maintains a more stable C_2 selectivity in the former. Speculating that the direct interaction of the La_2O_3 with the Na_2WO_4 is promoting the deactivation, we analyzed the spent La_2O_3 -NaWSi_0.8m using PXRD, as shown in Figure S3a. From the XRD data, we noticed that the Na_2WO_4 disappeared completely (after 14 h on stream), the peaks associated with the $\text{La}(\text{OH})_3$ phase diminished, and a new inactive $\text{NaLa}(\text{WO}_4)_2$ phase emerged, as shown in Figure S3. These peaks were found to be mild in the La/MgO-MnNaWSi_0.1m catalyst, as shown in Figure S4. The formation of this phase was previously reported by Matras et al. using a La-containing membrane reactor [40]. These results clearly show the instability of the La_2O_3 when in direct contact with the Na_2WO_4 . Presumably, in the work of Zou et al., the effect of Na_2WO_4 -induced deactivation was not evident, which was likely masked by the use of much larger amounts of catalysts, as we previously reported for the MnNaWSi catalyst [15]. Importantly, no such interactions were evidenced for MgO and Na_2WO_4 . To further monitor the deactivation process, we examined the HR-SEM images of bulk La_2O_3 , La/MgO, and MnNaWSi, as shown in Figure S5. The images clearly show that the spent La/MgO in the presence of the MnNaWSi phase undergoes sintering. Notably, the XRD data in Figures S3 and S4 show that the La-MnNaWSi_0.1s is more prone to deactivate compared to the La/MgO-MnNaWSi_0.1s, which highlights the benefit of the MgO support.

To examine the effect of residence time on catalytic performance, we tested the La/MgO-MnNaWSi_0.1s catalyst under several GHSV values at a temperature below the melting temperature of Na_2WO_4 (675 °C), which also means that the MnNaWSi phase is inactive, and at 725 °C, where both catalyst domains are active, as shown in Figure 3. Interestingly, at 725 °C, increasing the residence time (lower GHSV) did not significantly affect the methane conversion, C_2 selectivity, or C_2 yield, whereas the O_2 conversion showed a consistent decrease. It can therefore be concluded that the trend seen in CH_4 conversion at 725 °C is attributed to active site saturation at all tested GHSV values.

At 675 °C, we find that the C_2 selectivity and C_2 yield increased with GHSV. The CH_4 conversion remained similar at 20 and 40 $\text{L/g}_{\text{cat}}/\text{h}$ and increased slightly at 60 and 80 $\text{L/g}_{\text{cat}}/\text{h}$. Moreover, the C_2 selectivity was found to increase monotonically while the O_2 conversion decreased with the increase in GHSV. It is noted that the MnNaWSi catalyst is largely inactive at 675 °C (Figure 1a). To better understand the catalytic behavior of the stacked catalysts below the melting temperature of Na_2WO_4 , we tested the bare La/MgO and MnNaWSi at the same GHSV values, keeping the stacked structure of the catalyst bed and its size the same while replacing one of the domains with quartz particles, as shown in Figure S6. Consistently, we find that in all the tested GHSV values, the activity, selectivity, and yield of the La/MgO-MnNaWSi_0.1s were much higher than the respective levels in the stacked single component bed of La/MgO and MnNaWSi. The stacked MnNaWSi alone was found to mildly consume both methane and O_2 with no measurable formation of C_2 products. We find that decrease in O_2 conversion of the La/MgO-MnNaWSi_0.1s catalyst as a function of GHSV is correlated to that of the La/MgO. In contrast, the stacked La/MgO showed a decrease in C_2 selectivity, whereas the La/MgO-MnNaWSi_0.1s showed an increase in C_2 selectivity and yield with the increase in GHSV. It is postulated that the high reactivity of the La/MgO phase leads to the depletion of oxygen in the upper part of

the bed. Hence, the generated methyl radicals and ethane are channeled to the bottom part of the catalyst bed, which, as previously reported [14,41,42] and shown here in Figure S6, affords the higher C₂ selectivity under lean oxygen conditions.

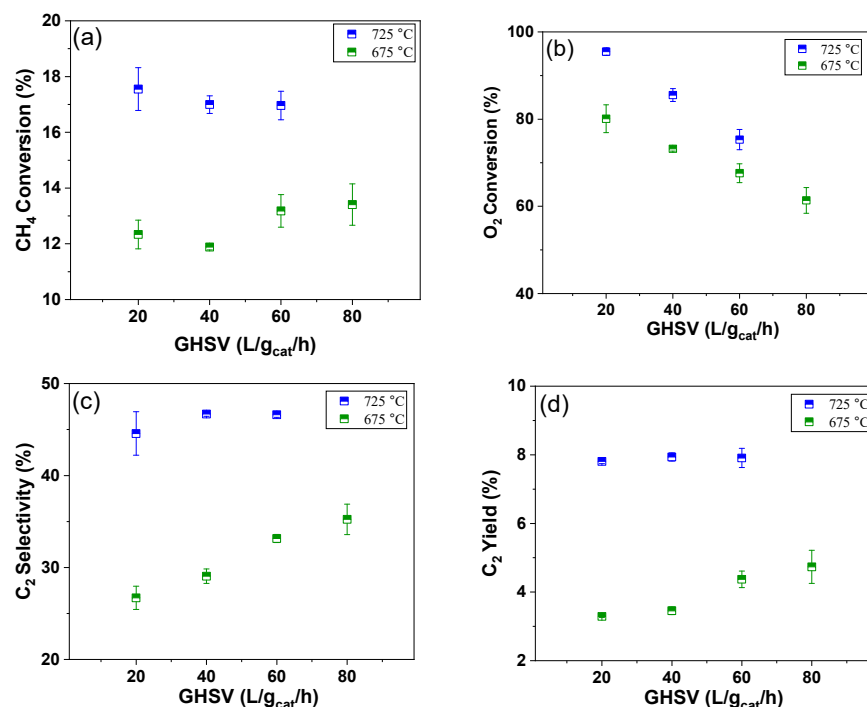


Figure 3. Analysis of La/MgO-MnNaWSi_{0.1s} at 725 °C and at 675 °C: (a) CH₄ conversion; (b) O₂ conversion; (c) C₂ selectivity; and (d) C₂ yield. Reaction conditions: 50 mg catalyst; catalyst bed 5 mm; molar ratio of CH₄:O₂:N₂:Ar = 4:1:1:4, and P ~ 1.3 bar. Each point is an average of data collected over 4 h of reaction, with the error bars representing the standard deviation.

The trends above strongly indicate that the two catalyst domains “communicate” to affect the kinetic mechanism. This observation is further supported by looking at the change in C₂H₄/C₂H₆ ratio as a function of temperature, as shown in Figure 4. We observe that above 700 °C, when the MnNaWSi becomes significantly active, the ratio starts to deviate from that obtained by the La/MgO catalyst to align with that of the MnNaWSi at 750 °C.

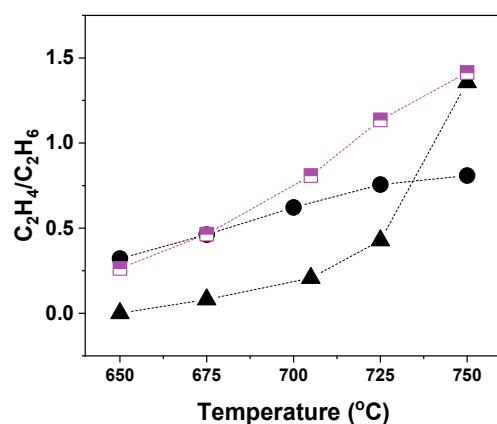


Figure 4. C₂H₄ to C₂H₆ ratio as a function of temperature (650–750 °C) for La/MgO-MnNaWSi_{0.1s}, La/MgO, and MnNaWSi.

To evaluate the effect of the transport of ethane and methyl radicals between the two catalyst phases, we tested the effect of catalytic bed composition with different mass ratio mechanical mixing (instead of stacking), as shown in Figure 5. Interestingly, the catalysts

with the higher bed fractions of La/MgO (20 wt.% and 50 wt.%) showed higher and more stable oxygen consumption in conjunction with a proportionally lower C₂ selectivity and, in turn, a lower C₂ yield. Overall, the 10 wt.% stacked catalyst showed both the highest and most stable C₂ selectivity and C₂ yield with TOS. With the increase in the bed volume to 20 wt.% and 50 wt.% we find that the C₂ selectivity drops. The drop in selectivity and, in turn, the C₂ yield is attributed to the short lifetime of methyl radicals [43], which most likely terminated before traversing to the bottom domain of the catalytic bed. This observation is further supported by the likeliness of the catalytic performance between the La/MgO-MnNaWSi_{0.5s} and the La/MgO-only bed. Explicitly, in the two catalyst bed compositions, the La/MgO dominated the catalytic performance, and the MnNaWSi was barely active in the test. The mechanically mixed 10 wt.% catalyst bed (La/MgO-MnNaWSi_{0.1m}) demonstrated low catalytic performance, similar to that of the MnNaWSi, as shown in Figure 5. Moreover, the mixed catalyst shows a drop in the catalytic activity and selectivity with TOS, which highlights the continuous occurrence of La₂O₃ deactivation due to interaction with the molten Na₂WO₄ phase, as previously reported for other oxides as well [15].

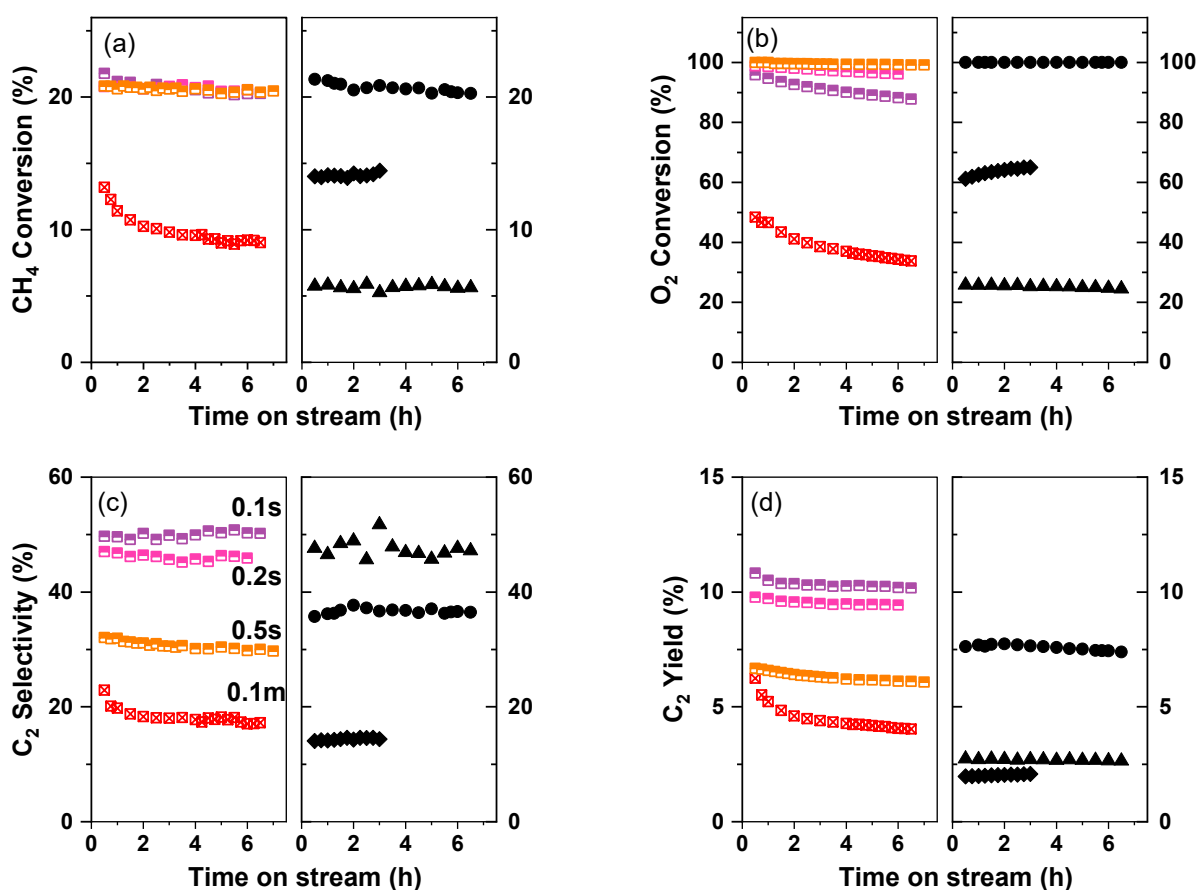


Figure 5. Catalytic performance with different La/MgO and MnNaWSi bed compositions at 725 °C. (a) CH₄ conversion; (b) O₂ conversion; (c) C₂ selectivity; (d) C₂ yield. ■ La/MgO-MnNaWSi_{0.1s}, ■ La/MgO-MnNaWSi_{0.2s}, ■ La/MgO-MnNaWSi_{0.5s}, ⊠ La/MgO-MnNaWSi_{0.1m}, ● La/MgO, ▲ MnNaWSi, and ◆ MgO.

Plotting the C₂ yield vs. the ethylene/ethane ratio at 725 °C for all the catalysts in this work, we find that the efficient stacking of the catalysts promotes both a higher C₂ yield and a higher olefin-to-paraffin ratio, as shown in Figure 6. Interestingly, we find that the increase in the La/MgO amount, in the La/MgO-MnNaWSi_xs (x = 0.1, 0.2, 0.5) catalyst bed is a correlated to a decrease in both the C₂ yield and the C₂H₄/C₂H₆ ratio with the La/MgO-MnNaWSi_{0.5s} nearing those of the mixed-bed La/MgO-MnNaWSi_{0.1m}. The

mechanical mixing of the two catalysts leads to relatively low C_2 yield and low C_2H_4/C_2H_6 ratios. Both of these trends are attributed to the deactivation process, as discussed above. Under lean oxygen conditions, Yoon et al. demonstrated that the conversion of ethane to ethylene occurs over surface lattice oxygens in MnNaWSi [41]. This coincides well with the higher C_2H_4/C_2H_6 ratios measured for the stacked beds. In these cases, the depletion of gas-phase oxygen in the top part of the bed results in the promotion of OCM in the bottom part of the bed under lean oxygen conditions, as opposed to the joint consumption of oxygen in the mixed catalyst bed.

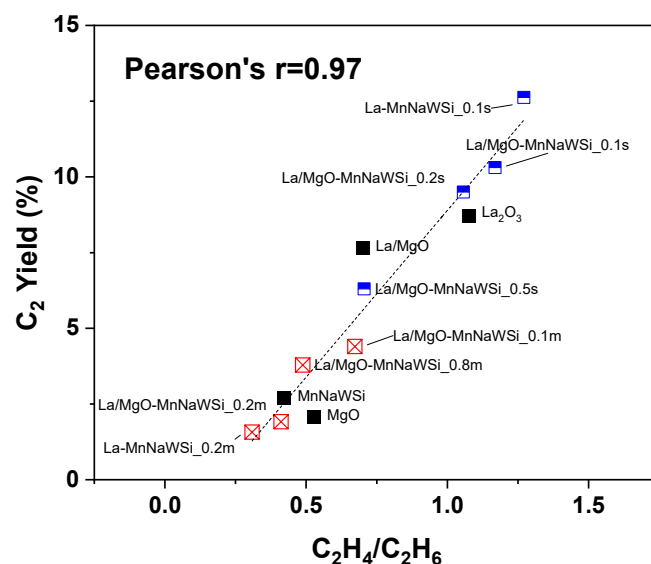


Figure 6. Pearson's correlation between the C_2 yield and the ratio of selectivity ratio of C_2H_4/C_2H_6 for all the catalytic tests at 725 °C. \boxtimes Mixed, \blacksquare Stacked, and \blacksquare Single components.

4. Conclusions

In this work, we demonstrate the promotion of OCM over a dual-domain catalyst bed composed of a La/MgO catalyst and the MnNaWSi catalyst. We show that the OCM mechanism is better promoted when the bed is composed of only 10 wt.% La/MgO stacked on top of 90 wt.% MnNaWSi (La/MgO-MnNaWSi_0.1s). Testing the latter bed composition at ~650 °C and 60 L/g_{cat}/h, we obtain ~10% CH₄ conversion and ~19% C₂ selectivity, whereas the MnNaWSi alone is inactive, and the La/MgO gives only 13% selectivity. Increasing the temperature to ~705 °C, the La/MgO-MnNaWSi_0.1s catalyst is found to give ~six-fold higher activity compared to the MnNaWSi catalyst or similar compared to the La/MgO catalyst, while the selectivity of the La/MgO-MnNaWSi_0.1s was 41%, which is higher than both individual catalysts. We further find that increasing the portion of the La/MgO or mixing it with the MnNaWSi showed diminished OCM performance, which is attributed to the deactivation of the La₂O₃ by reaction with the Na₂WO₄. Finally, we show that the dual-domain catalyst bed is promoting OCM through a synergistic kinetic mechanism that is active even below 700 °C.

Supplementary Materials: The following supporting information can be downloaded at: <https://www.mdpi.com/article/10.3390/chemistry5020075/s1>, Figure S1: XRD patterns for the original catalysts, (a) La/MgO; (b) La₂O₃ (after exposure to ambient air); (c) La₂O₃(fresh); (d) MnNaWSi; Figure S2: Catalytic performance of La₂O₃ or La/MgO bed stacking over MnNaWSi bed at 725 °C; Figure S3: XRD patterns: (a) Spent La₂O₃-NaWSi_0.8m bed reacted for 14 h at 675–725 °C; (b) Fresh NaWSi catalyst; (c) Fresh La₂O₃ catalyst; Figure S4: XRD patterns: (a) Spent La/MgO-MnNaWSi_0.1m bed, reacted for 14 h at 725–750 °C; (b) Fresh MnNaWSi catalyst; (c) Fresh La/MgO catalyst; Figure S5: HR-SEM images of fresh and spent catalysts: (a) fresh bulk La₂O₃; (b) Spent La₂O₃; (c) fresh La/MgO; (d) Spent La/MgO; (e) fresh MnNaWSi; (f) spent MnNaWSi; (g) spent La/MgO-MnNaWSi_0.1s; (h) spent La/MgO-MnNaWSi_0.1m; Figure S6: Catalytic performance over

a range of GHSV (20–80 L g⁻¹ h⁻¹) Table S1: Compositions of different pure catalysts.; Table S2: Expected catalytic performance of stacked 10 wt% catalyst based on performance of single components and their mass composition.

Author Contributions: Conceptualization, B.H., J.W., D.S. and O.M.G.; software, B.H.; methodology, B.H.; validation, B.H. and O.M.G.; formal analysis, B.H., J.W. and D.S.; investigation, B.H.; resources, O.M.G.; data curation, B.H., J.W. and O.M.G.; writing—original draft preparation, B.H.; writing—review and editing, B.H., J.W., D.S. and O.M.G.; visualization, B.H.; supervision, O.M.G.; project administration, O.M.G.; funding acquisition, O.M.G. All authors have read and agreed to the published version of the manuscript.

Funding: The generous supported of the Binational Industrial Research and Development (BIRD) foundation (Grant number 716613) is gratefully acknowledged.

Data Availability Statement: Not applicable.

Acknowledgments: The financial support of the Grand Technion Energy Program and the Russell Berrie Nanotechnology Institute is also acknowledged. The author B.H. acknowledges the financial support of the Energean Excellence Scholarship.

Conflicts of Interest: The authors declare no conflict of interest.

References

1. Keller, G.E.; Bhasin, M.M. Synthesis of Ethylene via Oxidative Coupling of Methane. I. Determination of Active Catalysts. *J. Catal.* **1982**, *73*, 9–19. [[CrossRef](#)]
2. Galadima, A.; Muraza, O. Revisiting the Oxidative Coupling of Methane to Ethylene in the Golden Period of Shale Gas: A Review. *J. Ind. Eng. Chem.* **2016**, *37*, 1–13. [[CrossRef](#)]
3. Weiland, P. Biogas Production: Current State and Perspectives. In *Applied Microbiology and Biotechnology*; Springer: Berlin/Heidelberg, Germany, 2010; pp. 849–860. [[CrossRef](#)]
4. Kiani, D.; Sourav, S.; Baltrusaitis, J.; Wachs, I.E. Oxidative Coupling of Methane (OCM) by SiO₂-Supported Tungsten Oxide Catalysts Promoted with Mn and Na. *ACS Catal.* **2019**, *9*, 5912–5928. [[CrossRef](#)]
5. Arndt, S.; Otremba, T.; Simon, U.; Yildiz, M.; Schubert, H.; Schomäcker, R. Mn-Na₂WO₄/SiO₂ as Catalyst for the Oxidative Coupling of Methane. What Is Really Known? *Appl. Catal. A Gen.* **2012**, *425–426*, 53–61. [[CrossRef](#)]
6. Xueping, F.; Shuben, L.; Jingzhi, L.; Yanlai, C. Oxidative Coupling of Methane on W-Mn Catalysts. *J. Mol. Catal.* **1992**, *6*, 427–433.
7. Kiani, D.; Sourav, S.; Wachs, I.E.; Baltrusaitis, J. Synthesis and Molecular Structure of Model Silica-Supported Tungsten Oxide Catalysts for Oxidative Coupling of Methane (OCM). *Catal. Sci. Technol.* **2020**, *10*, 3334–3345. [[CrossRef](#)]
8. Li, S.B. Oxidative Coupling of Methane over W-Mn/SiO₂ Catalyst. *Chin. J. Chem.* **2001**, *19*, 16–21. [[CrossRef](#)]
9. Wang, D.J.; Rosynek, M.P.; Lunsford, J.H. Oxidative Coupling of Methane over Oxide-Supported Sodium-Manganese Catalysts. *J. Catal.* **1995**, *155*, 390–402. [[CrossRef](#)]
10. Werny, M.J.; Wang, Y.; Girgsdies, F.; Schlögl, R.; Trunschke, A. Fluctuating Storage of the Active Phase in a Mn-Na₂WO₄/SiO₂ Catalyst for the Oxidative Coupling of Methane. *Angew. Chem.* **2020**, *132*, 15031–15036. [[CrossRef](#)]
11. Sinev, M.; Ponomareva, E.; Sinev, I.; Lomonosov, V.; Gordienko, Y.; Fattakhova, Z.; Shashkin, D. Oxygen Pathways in Oxidative Coupling of Methane and Related Processes. Case Study: NaWMn/SiO₂ Catalyst. *Catal. Today* **2019**, *333*, 36–46. [[CrossRef](#)]
12. Hayek, N.S.; Lucas, N.S.; Warwar Damouny, C.; Gazit, O.M. Critical Surface Parameters for the Oxidative Coupling of Methane over the Mn-Na-W/SiO₂ Catalyst. *ACS Appl. Mater. Interfaces* **2017**, *9*, 40404–40411. [[CrossRef](#)]
13. Huang, B.; Hayek, N.S.; Sun, G.; Mottaghi-Tabar, S.; Simakov, D.S.A.; Gazit, O.M. Correlating Properties of the Mn₂O₃-Na₂WO₄/SiO₂ Catalyst with Statistically Estimated Parameters for the Oxidative Coupling of Methane. *Energy Fuels* **2021**, *35*, 9589–9598. [[CrossRef](#)]
14. Pak, S.; Qiu, P.; Lunsford, J.H. Elementary Reactions in the Oxidative Coupling of Methane over Mn/Na₂WO₄/SiO₂ and Mn/Na₂WO₄/MgO Catalysts. *J. Catal.* **1998**, *179*, 222–230. [[CrossRef](#)]
15. Hayek, N.S.; Khlief, G.J.; Horani, F.; Gazit, O.M. Effect of Reaction Conditions on the Oxidative Coupling of Methane over Doped MnOx-Na₂WO₄/SiO₂ Catalyst. *J. Catal.* **2019**, *376*, 25–31. [[CrossRef](#)]
16. Lomonosov, V.I.; Sinev, M.Y. Oxidative Coupling of Methane: Mechanism and Kinetics. *Kinet. Catal.* **2016**, *57*, 647–676. [[CrossRef](#)]
17. Martin, G.A.; Mirodatos, C. Surface Chemistry in the Oxidative Coupling of Methane. *Fuel Process. Technol.* **1995**, *42*, 179–215. [[CrossRef](#)]
18. Horn, R.; Schlögl, R. Methane Activation by Heterogeneous Catalysis. *Catal. Lett.* **2015**, *145*, 23–39. [[CrossRef](#)]
19. Campbell, K.D.; Lunsford, J.H. Contribution of Gas-Phase Radical Coupling in the Catalytic Oxidation of Methane. *J. Phys. Chem.* **1988**, *92*, 5792–5796. [[CrossRef](#)]
20. Tong, Y.; Rosynek, M.P.; Lunsford, J.H. Secondary Reactions of Methyl Radicals with Lanthanide Oxides: Their Role in the Selective Oxidation of Methane. *J. Phys. Chem.* **1989**, *93*, 2896–2898. [[CrossRef](#)]

21. Zhou, Q.; Wang, Z.Q.; Li, Z.; Wang, J.; Xu, M.; Zou, S.; Yang, J.; Pan, Y.; Gong, X.Q.; Xiao, L.; et al. CH₃•-Generating Capability as a Reactivity Descriptor for Metal Oxides in Oxidative Coupling of Methane. *ACS Catal.* **2021**, *11*, 14651–14659. [[CrossRef](#)]
22. Lin, C.H.; Campbell, K.D.; Wang, J.X.; Lunsford, J.H. Oxidative Dimerization of Methane over Lanthanum Oxide. *J. Phys. Chem.* **1986**, *90*, 534–537. [[CrossRef](#)]
23. Wu, J.; Zhang, H.; Qin, S.; Hu, C. La-Promoted Na₂WO₄/Mn/SiO₂ Catalysts for the Oxidative Conversion of Methane Simultaneously to Ethylene and Carbon Monoxide. *Appl. Catal. A Gen.* **2007**, *323*, 126–134. [[CrossRef](#)]
24. Ismagilov, I.Z.; Matus, E.V.; Vasil'Ev, S.D.; Kuznetsov, V.V.; Kerzhentsev, M.A.; Ismagilov, Z.R. Oxidative Condensation of Methane in the Presence of Modified MnNaW/SiO₂ Catalysts. *Kinet. Catal.* **2015**, *56*, 456–465. [[CrossRef](#)]
25. Ghose, R.; Hwang, H.T.; Varma, A. Oxidative Coupling of Methane Using Catalysts Synthesized by Solution Combustion Method: Catalyst Optimization and Kinetic Studies. *Appl. Catal. A Gen.* **2014**, *472*, 39–46. [[CrossRef](#)]
26. Zhao, M.; Ke, S.; Wu, H.; Xia, W.; Wan, H. Flower-like Sr-La₂O₃ Microspheres with Hierarchically Porous Structures for Oxidative Coupling of Methane. *Ind. Eng. Chem. Res.* **2019**, *58*, 22847–22856. [[CrossRef](#)]
27. Hou, Y.H.; Han, W.C.; Xia, W.S.; Wan, H.L. Structure Sensitivity of La₂O₂CO₃ Catalysts in the Oxidative Coupling of Methane. *ACS Catal.* **2015**, *5*, 1663–1674. [[CrossRef](#)]
28. Noon, D.; Seubsai, A.; Senkan, S. Oxidative Coupling of Methane by Nanofiber Catalysts. *ChemCatChem* **2013**, *5*, 146–149. [[CrossRef](#)]
29. Song, J.; Sun, Y.; Ba, R.; Huang, S.; Zhao, Y.; Zhang, J.; Sun, Y.; Zhu, Y. Monodisperse Sr-La₂O₃ Hybrid Nanofibers for Oxidative Coupling of Methane to Synthesize C₂ Hydrocarbons. *Nanoscale* **2015**, *7*, 2260–2264. [[CrossRef](#)]
30. Jaroenpanon, K.; Tiyyatha, W.; Chuksaw, T.; Sringam, S.; Witoon, T.; Wattanakit, C.; Chareonpanich, M.; Faungnawakij, K.; Seubsai, A. Synthesis of Na₂WO₄-MnxOy Supported on SiO₂ or La₂O₃ as Fiber Catalysts by Electrospinning for Oxidative Coupling of Methane: Synthesis of Na₂WO₄-MnxOy Supported on SiO₂ or La₂O₃ as Fiber Catalysts. *Arab. J. Chem.* **2022**, *15*, 103577. [[CrossRef](#)]
31. Zou, S.; Li, Z.; Zhou, Q.; Pan, Y.; Yuan, W.; He, L.; Wang, S.; Wen, W.; Liu, J.; Wang, Y.; et al. Surface Coupling of Methyl Radicals for Efficient Low-Temperature Oxidative Coupling of Methane. *Chin. J. Catal.* **2021**, *42*, 1117–1125. [[CrossRef](#)]
32. Rollins, B.; Grosjean, N.; Poulston, S. The Impact of the Presence of Various Relevant Gases during Aging of MnNa₂WO₄/SiO₂ Catalyst on Its Performance for the Oxidative Coupling of Methane. *Appl. Catal. A Gen.* **2020**, *598*, 117606. [[CrossRef](#)]
33. Hayek, N.S.; Lucas, N.S.; Warwar Damouny, C.; Gazit, O.M. A Comparative Study of Precursor Effect on Manganese Post-Synthetic Incorporation into the T-Sites of Dealuminated B-Zeolite. *Microporous Mesoporous Mater.* **2017**, *244*, 31–36. [[CrossRef](#)]
34. Haibel, E.; Berendts, S.; Walter, D. Thermogravimetric and X-ray Diffraction Investigation on Carbonated Lanthanum Oxide and Lanthanum Hydroxide Formed in Humid CO₂ Atmosphere. *J. Therm. Anal. Calorim.* **2018**, *134*, 261–267. [[CrossRef](#)]
35. Sadjadi, S.; Jašo, S.; Godini, H.R.; Arndt, S.; Wollgarten, M.; Blume, R.; Görke, O.; Schomäcker, R.; Wozny, G.; Simon, U. Feasibility Study of the Mn-Na₂WO₄/SiO₂ Catalytic System for the Oxidative Coupling of Methane in a Fluidized-Bed Reactor. *Catal. Sci. Technol.* **2015**, *5*, 942–952. [[CrossRef](#)]
36. Hiyoshi, N.; Ikeda, T. Oxidative Coupling of Methane over Alkali Chloride-Mn-Na₂WO₄/SiO₂ Catalysts: Promoting Effect of Molten Alkali Chloride. *Fuel Process. Technol.* **2015**, *133*, 29–34. [[CrossRef](#)]
37. Gordienko, Y.; Usmanov, T.; Bychkov, V.; Lomonosov, V.; Fattakhova, Z.; Tulenin, Y.; Shashkin, D.; Sinev, M. Oxygen Availability and Catalytic Performance of NaWMn/SiO₂ Mixed Oxide and Its Components in Oxidative Coupling of Methane. *Catal. Today* **2016**, *278*, 127–134. [[CrossRef](#)]
38. Matras, D.; Vamvakeros, A.; Jacques, S.D.M.; Grosjean, N.; Rollins, B.; Poulston, S.; Stenning, G.B.G.; Godini, H.R.; Drnec, J.; Cernik, R.J.; et al. Effect of Thermal Treatment on the Stability of Na-Mn-W/SiO₂ catalyst for the Oxidative Coupling of Methane. *Faraday Discuss.* **2021**, *229*, 176–196. [[CrossRef](#)]
39. Pak, S.; Lunsford, J.H. Thermal Effects during the Oxidative Coupling of Methane over Mn/Na₂WO₄/SiO₂ and Mn/Na₂WO₄/MgO Catalysts. *Appl. Catal. A Gen.* **1998**, *168*, 131–137. [[CrossRef](#)]
40. Vamvakeros, A.; Matras, D.; Jacques, S.D.M.; di Michiel, M.; Middelkoop, V.; Cong, P.; Price, S.W.T.; Bull, C.L.; Senecal, P.; Beale, A.M. Real-Time Tomographic Diffraction Imaging of Catalytic Membrane Reactors for the Oxidative Coupling of Methane. *Catal. Today* **2021**, *364*, 242–255. [[CrossRef](#)]
41. Yoon, S.; Lim, S.; Choi, J.W.; Suh, D.J.; Song, K.H.; Ha, J.M. Study on the Unsteady State Oxidative Coupling of Methane: Effects of Oxygen Species from O₂, Surface Lattice Oxygen, and CO₂ on the C²⁺ Selectivity. *RSC Adv.* **2020**, *10*, 35889–35897. [[CrossRef](#)]
42. Tiemersma, T.P.; Tuinier, M.J.; Gallucci, F.; Kuipers, J.A.M.; Annaland, M.V.S. A Kinetics Study for the Oxidative Coupling of Methane on a Mn/Na₂WO₄/SiO₂ Catalyst. *Appl. Catal. A Gen.* **2012**, *433–434*, 96–108. [[CrossRef](#)]
43. Jones, C.A.; Leonard, J.J.; Sofranko, J.A. The Oxidative Conversion of Methane to Higher Hydrocarbons over Alkali-Promoted MnSiO₂. *J. Catal.* **1987**, *103*, 311–319. [[CrossRef](#)]

Disclaimer/Publisher's Note: The statements, opinions and data contained in all publications are solely those of the individual author(s) and contributor(s) and not of MDPI and/or the editor(s). MDPI and/or the editor(s) disclaim responsibility for any injury to people or property resulting from any ideas, methods, instructions or products referred to in the content.